RESEARCH ARTICLE

Utilizing Artificial Neural Networks and Combined Capacitance-Based Sensors to Predict Void Fraction in Two-Phase Annular Fluids Regardless of Liquid Phase Type

MUSTAFA A. AL-FAYOUMI[1], HANI MAHMOUD AL-MIMI[2], ARYAN VEISI[3], HUSSAIN AL-AQRABI[4], MOHAMMAD SH. DAOUD[5], AND EHSAN EFTEKHARI-ZADEH[6]

[1]Department of Cybersecurity, King Hussein School of Computing Sciences, Princess Sumaya University for Technology (PSUT), Amman 11941, Jordan
[2]Department of Cybersecurity, Al-Zaytoonah University of Jordan, Amman 11733, Jordan
[3]Department of Electrical Engineering, Kermanshah University of Technology, Kermanshah 6715685420, Iran
[4]Department of Computer Information Science, Higher Colleges of Technology, Sharjah, United Arab Emirates
[5]College of Engineering, Al Ain University, Abu Dhabi, United Arab Emirates
[6]Institute of Optics and Quantum Electronics, Abbe Center of Photonics, Friedrich Schiller University Jena, 07743 Jena, Germany

Corresponding author: Ehsan Eftekhari-Zadeh (e.eftekharizadeh@uni-jena.de)

ABSTRACT Assessing the void fraction in diverse multiphase flows across industries, including petrochemical, oil, and chemical sectors, is crucial. There are multiple techniques available for this objective. The capacitive sensor has gained significant popularity among these methods and has been extensively utilized. Fluid properties have a substantial impact on the performance of capacitance sensors. Factors such as density, pressure, and temperature can introduce significant errors in void fraction measurements. One approach to address this issue is a meticulous and laborious routine calibration process. In the current study, an artificial neural network (ANN) was developed to accurately Assess the proportion of gas in a biphasic fluid motion, irrespective of variations in the fluid phase form or variations, eliminating the need for frequent recalibration. To achieve this objective, novel combined capacitance-based sensors were specifically designed. The sensors were simulated by employing the COMSOL Multiphysics application. The simulation encompassed five distinct liquids: oil, diesel fuel, gasoline, crude oil, and water. The input for training a multilayer perceptron network (MLP) came from data gathered through COMSOL Multiphysics, simulations for estimating the Percentage of gas content of an annular two-phase fluid with a specific liquid form. The MATLAB software was utilized to construct and model the proposed neural network. The utilization of the novel and precise apparatus for measuring the intended MLP model demonstrated the ability to prognosticate the volume percentage with a mean absolute error (MAE) of 0.004.

INDEX TERMS Ring-type electrode, TRFLC electrode, concave-type electrode, multiphase flow, annular flow, artificial intelligence, capacitive sensor, sensitivity.

I. INTRODUCTION

Industries encompass a diverse range of two-phase fluids, including oil-air, oil-water, and water-air combinations.

The associate editor coordinating the review of this manuscript and approving it for publication was Alon Kuperman.

These fluid combinations are prevalent across various sectors, acting as petrochemical, chemical, oil, and gas industries [1]. One out of the prevailing and significant concerns in the mentioned fields today revolves around accurately predicting the void fraction in interwoven fluids [2]. It is worth noting that flow metering of fluids holds importance in

various other areas. This includes controlling procedures, financial measuring, and managing repositories. However, measuring the flow of two-phase fluids, known for their inherent complexity, such as oil-gas or oil-water mixtures, proves challenging [3]. The common technique for gauging the flow of every individual stage in pipelines involves first separating the mixed phases and then calculating the flow rate of each phase separately. However, this approach comes with challenges, including being time-consuming and costly [4]. Hence, the design and production of flow meters offer numerous advantages, including the ability to detect flow type, measure void fraction, and perform these tasks seamlessly without interrupting the procedure [5], [6]. The volume percentage in a gas (or air)–liquid-phase fluid has the potential to be calculated in between the air volume within the tube through the total cross-sectional area of the tube. Several nondestructive methods exist for determining the void fraction, ranging from references [7], [8], [9], [10], and [11]. Capacitive detectors offer a suitable method for measuring the gas percentage without the need to interrupt the process or separate the phases. Electrodes play a critical role in capacitance-based sensors, and their arrangement greatly influences the precision of measurement. The choice of electrode configuration, such as concave, ring, and helix, is directly linked to the form of fluid in the tube. Several studies have concentrated on the three primary flows (stratified, annular, and homogeneous) present in a pipe for a biphasic fluid motion. For instance, the concave electrode configuration has been suggested for accurately measuring a conductive two-liquid-phase flow [12], [13], [14], [15], [16], [17]. Li et al. conducted a study [18] examining the measurement error of capacitive sensors. In a study carried out by Hammer et al. [19], they examined a two oil-water phase flow regime and observed that capacitance-based sensors using straight electrode surfaces had limitations in terms of their dependence on flow regime and distribution. They found that accurate outcomes could only be achieved when the elements were comprehensively mixed. If the volume of the foams was slighter than the section of the substance, the resultant combination exhibited a predominantly homogeneous nature. The analysis carried out by Jaworek et al. [20] focused on a two-phase water-air flow and investigated the performance of a total of five distinct arrangements (including helix-shape, concave, and double-ring) in capacitance sensors. The findings revealed that the concave shape exhibited the uppermost sensitivity. Additionally, earlier findings have explored the sensibility of capacitance-based gauges in Unique kinds of two-phase flows. In a study referenced as [21], it was remarked that the concave-shaped arrangement demonstrated the uppermost susceptibility in a biphasic fluid motion, whereas the two-ring-shaped configuration exhibited the lowermost susceptibility. Sarkis et al. conducted a study [22] focusing on air-solid multiphase flow. Sami et al. accomplished investigations on non-conducting liquid-air(gas) flow, where they used six altered capacitance-based sensors. The study

demonstrated that the helical conductor had the utmost sensitivity for oil-gas biphasic fluid motion, whereas the concave electrode was found to be the most accurate for the annular flow regime [23]. Ahmed conducted a revision [24] on a two-phase gas-oil fluid flowing Over the course of a flat tube using a capacitive sensor. The study assessed the sensor's sensitivity by utilizing concave and ring electrodes and found that in the same blade size, the ring type had superior sensitivity. However, the study also identified the configuration type as a limitation to precisely deciding the void fraction. In a study conducted by Nazemi et al. [25], the effectiveness of two frequently used sensors in the measurement of multiphase flow was compared: capacitance-based electrode and gamma-ray attenuation-based. The sensors underwent testing in an annular flow consisting of gas and oil, with their momentary sensitivity being assessed at different void fractions. The outcomes indicated that the concave capacitance-based sensor performed superior in volume percentages between 0.8 and 1. Wang et al. [26] used three special capacitance-based sensors: two-ring, array, and concave sensors. Their investigation focused on analyzing the gas percentage in a multiphase fluid and predicting the corresponding flow regime based on the collected data. Krupa and colleagues [27] utilized a capacitive sensor, for instance, the concave-shape configuration, to gauge the air fraction in slight channels with diameters less than 1 cm. A high-rate oscillator's frequency deviation was utilized by them and coupled the capacitance sensor to an oscillatory circuit with parallel inductance to calculate the gas fraction in a two-phase flow. Chen et al. [28] employed a probe based on multi-wire capacitance in their study to gauge the volume percentage in a stratified gas-liquid pattern. This probe, based on the single-wire capacitance-based probe, enabled the measurement of both mean and specific gas percentages by assessing the liquid level at different positions along the tube. According to reference [29], artificial intelligence (AI) is widely utilized within the industrial sector as a prevalent and frequently employed approach. Artificial Neural Networks (ANNs) have gained significant prominence as a powerful tool with diverse applications in various fields. They have found extensive use in disciplines such as electrical engineering [30], [31], [32], [33], control engineering [34], [35], and Instrumentation [36], [37], [38], [39]. A comprehensive review of capacitive sensors in the domain of multiphase flow measurement and imaging was conducted by Aluisio do Nascimento Wrasse et al., shedding light on their diverse applications [40]. Drawing inspiration from the pioneering research conducted by Zhihong Huang and colleagues, electrical capacitance sensors with various geometries were developed and tested to optimize two-phase flow monitoring. The observed sensitivity variations with changing oil content closely align with their prior findings [41]. Zhuoqun Xu et al. employ flow pattern images to enhance the accuracy of predicting oil and gas flow rates in two-phase flow, using a Convolutional Neural Network (CNN) model, while acknowledging the computational challenges and emphasizing the need for future research into

lightweight and embedded models for real-time industrial applications [42]. Vendruscolo et al. introduce a flexible PCB-based capacitive array sensor for direct imaging of two-phase flows, effectively characterizing flow patterns based on fluid permittivity differences, with future potential for quantitative flow analysis [43]. Lusheng Zhai established an equivalent circuit model for a concave capacitance sensor used in the measurement of stratified oil-water flow, optimizing its geometric structure based on excitation signal frequency effects. Additionally, a capacitance sensor system capable of detecting both the real and imaginary parts of oil-water complex admittance, as applied in dynamic experiments of horizontal oil-water flows, offers insights into how flow patterns and excitation frequency impact complex admittance measurements. The study emphasizes the importance of considering these factors for accurate water holdup measurements in horizontal oil-water flows [44]. Kim et al. introduce a capacitance sensor with asymmetric electrodes for void fraction measurement, accompanied by a novel calibration method addressing the nonlinear capacitance-void fraction relationship by integrating repeated capacitance measurements and bimodal temporal distributions, leading to a 2.99% relative error compared to a quick-closing valve (QCV) system and demonstrating the method's potential for reliable void fraction measurements under various conditions [45]. Obtaining oil products involves three steps: extracting crude oil and gas from oil wells, transporting them through transmission lines to refineries, and refining the products. A schematic view of this process can be found in Figure 1. The characteristics of gas-liquid two-phase flow patterns can give rise to different flow regimes, where the most common ones are stratified and annular. In stratified flow, the gas and liquid phases remain distinctly separated, with the gas phase typically occupying the upper portion while the liquid phase flows along the lower part of the conduit. On the other hand, annular flow is characterized by a thin liquid film lining the inner wall of the conduit, while the gas phase forms a core in the center. Figure 2 provides a visual demonstration of these two flow regimes. Fluid properties have a significant impact on the performance of capacitance sensors, with factors such as density, pressure, and temperature capable of inducing substantial errors in void fraction measurements. A potential solution to address this problem is an intervallic recalibration of the implementation, which can be a laborious task. Based on earlier studies in this area, the present investigation endeavors to propose a precise metering system capable of predicting the void fraction accurately, irrespective of the liquid type. COMSOL program was employed to model a two-annular-phase flow at various volume percentages to fulfill this objective. Our primary objective in this research was to improve the accuracy of void percentage prediction in biphasic fluid motion by integrating a capacitance-based sensor, referred to as a (TRFLC) sensor in reference [46], along with ring and concave sensors. These sensors' outputs were

then analyzed using an MLP neural network. The key focus of this study was to enhance the precision of the detection system by implementing a TRFLC capacitance-based sensor in conjunction with other sensors, such as the ring and concave types. This paper introduces a sophisticated technique based on artificial neural networks (ANN) for valuing the gas fraction in a multiphase flow independent of any changes in the liquid phase. The sensor was created by combining two popular sensors, the concave and ring, which were linked sequentially with the TRFLC capacitive sensor. To determine the gas percentages in an annular two-phase fluid that contains a particular liquid type, we utilized data from COMSOL Multiphysics as input to train an MLP model implemented in MATLAB software. Our MLP model, which was trained using data from an improved metering system, showed a low mean absolute error in predicting void fraction. In addition to the integration of multiple sensors and the utilization of MLP networks for sensor combinations, a novel contribution is made by our work through the incorporation of a systematic process for selecting one of the most accurate sensor combinations based on the Mean Absolute Error (MAE). This unique approach aims to address the challenge of optimizing sensor selection and fusing sensor data, ultimately improving the accuracy and reliability of our predictive model.
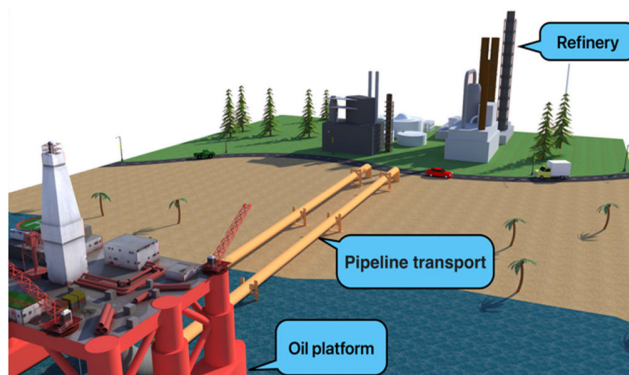

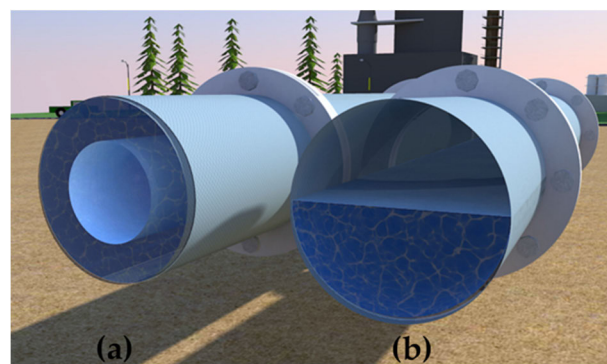**FIGURE 1.** The three vital steps in oil production - extraction, transportation, and refining.

FIGURE 2. Illustrated are two distinct fluid types - (a) annular and (b) stratified fluids.

II. VOID FRACTION MEASUREMENT TECHNIQUE

The arrangement or distribution of components within a flow, known as the geometric distribution, can have an impact on the rates of momentum, mass, and energy transfer. Furthermore, the flow behaviour within each component or phase is influenced by the flow regimes, which can be considered as a specific type of geometric distribution for the constituent [47]. In the context of this study, sensors have been utilized that employ electrical principles to measure capacitance accurately. This approach offers significant advantages, as it eliminates the need for invasive or physical contact methods, ensuring precision while minimizing potential risks. In multiphase flow, the dimensionless quantity of void fraction is regarded as the most crucial factor. Despite its initial usage dating back to the 1940s, void fraction remains relevant and continues to be employed in various applications to this day. Figure 3a has been included to present a visual depiction of the boundary layer properties within the annular cavity, offering a clear and informative illustration of these essential characteristics. In the context of multiphase flow, the term ''void fraction'' refers to the proportion of a geometric domain occupied by a different phase. This concept is depicted in Figure 3b, which illustrates various terminologies related to polyphase flow. Equations (1) and (2) were used to describe the phase fractions in the two-phase oil-gas regime during annular flow.

$$Vwater = \frac{\pi R1^2 - \pi R^2}{\pi R1^2} = \frac{R1^2 - R^2}{R1^2} \qquad (1)$$

$$Vgas = \frac{\pi R^2}{\pi R1^2} = \frac{R^2}{R1^2} \qquad (2)$$
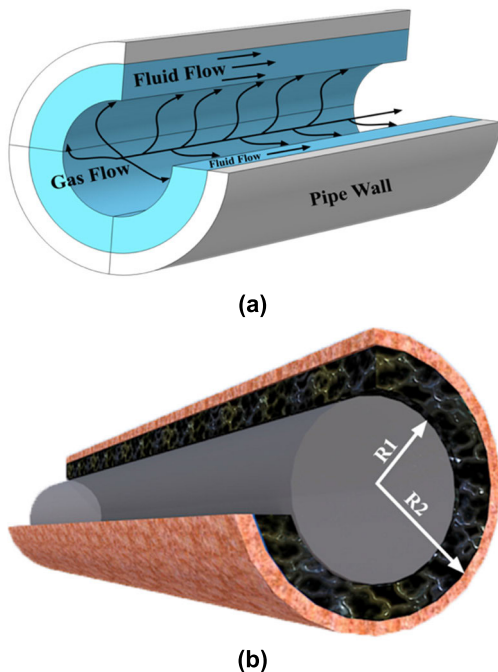

(a)

(b)

FIGURE 3. (a) Schematic view of boundary layer properties two-phase flow. (b) The construction of the annular flow arrangement is two-phase.

III. VALIDATION AND SIMULATIONS

This study focused on examining an annular configuration for a liquid film flow consisting of air and liquid. An annular flow regime occurs in a pipe when a gas or vapor flows through the center of the pipe while a thin film or annulus of liquid flows along the inner wall of the pipe. This regime typically occurs at high gas velocities and low liquid flow rates, resulting in a significant gas-liquid density difference. The liquid film in the annular flow regime is usually thin and continuous, with the gas phase occupying the majority of the pipe's cross-sectional area. The formation of an annular flow regime is influenced by factors such as fluid properties, flow rates, pipe diameter, and surface tension. Furthermore, it's worth mentioning that this flow pattern is often associated with, a distinct flow pattern in pipelines, is characterized by the concentric or ring-like movement of two phases: gas at the core and liquid forming an annular layer around it. This pattern is observed when a notably high gas-to-liquid ratio is maintained, the pipe geometry is conducive to this flow, and an adequate flow velocity is sustained. The presence of annular flow is recognized as crucial when multiphase fluid transportation systems are designed and operated, with particular relevance in sectors such as the oil and gas industry, as it significantly impacts pressure dynamics, flow rates, and heat transfer characteristics, influencing system efficiency and safety. In order to evaluate the performance of the COMSOL Multiphysics software, the authors utilized previously validated simulated data from their previous work [33]. The data involved the design and simulation of two commonly used electrocapacitive sensors, namely the concave and ring sensors. Therefore, the results obtained from this software are considered reliable and trustworthy. COMSOL Multiphysics is widely recognized as one of the most frequently employed software applications in various fields. This program leverages the finite element method (FEM) to create a specialized situation that enables simulation and analysis in various industries, encompassing fields such as petrochemical, mechanical, and electronic sectors. A gas region is formed during the simulation due to the presence of strong electric fields surrounding the plates of the simulated capacitor. As the space among the electrodes rises, the electrical field drops because it is conversely proportional to the cube of the distance. A three-dimensional model within the realm of electrostatic physics, specifically in the domain of AC/DC (Alternating Current/Direct Current) focusing on Electric Fields and Currents, was created. The simulation was conducted under the stationary regime, wherein variables associated with the electric field remained constant throughout the duration of the simulation. By utilizing a stationary study, the surrounding electrical field, which has the potential to grow indefinitely, becomes negligible. This is because the variables that impact the electrical field remain Invariable. As mentioned before, the COMSOL simulation platform utilizes the finite element method, known for its ability to provide precise results, in order to conduct simulations effectively. Multiple meshing techniques are available, and in

this case, the mesh size has been set to a finer resolution. In the COMSOL simulation platform, the designed structure is simulated and solved using the finite element method, utilizing a network of elements for accurate analysis and computations. By employing a finer mesh size, each element in the simulation is reduced in size, resulting in a higher level of accuracy in the results generated by the software. Table 1 provides the sizes of the various components within the finer mesh size. The computer utilized for the task was equipped with an Intel i5 4510U CPU and 8GB of RAM.

TABLE 1. Principal features of the smaller mesh size.

Characteristic's	Amount
The largest element dimension.	36 mm
The smallest element dimension.	2 mm
The highest rate of element size increase.	1.14
The curvature factor	0.21
The level of detail in confined regions.	0.88

A. MODELING AND ANALYZING A CONCAVE ELECTRODE IN COMSOL MULTIPHYSICS

The benchmarked software was utilized to simulate the concave sensor in this specific section. For the two-phase air-liquid annular flow regime, simulations were conducted multiple times (specifically, 21 repetitions) using a range of volume percentages from full (0) to empty (1), with an increment of 0.05. These simulations encompassed five distinct liquids: water, gasoline, diesel fuel, oil, crude oil, and air. The relative permittivity (εr) is the parameter that quantifies the reduction of the electric field between charges compared to that in a vacuum. At room temperature, the respective relative permittivity (εr) values for water, gasoline, diesel fuel, oil, crude oil, and air are 81, 2.7, 2.4, 2.2, 2, 1, respectively. Air content was considered in all of the simulations to account for the observable fringing fields surrounding the capacitor plates. Although these fields reduce conversely commensurate to the cube of the space, it is important to note that they have the prospective to approach infinity. To address this issue, A three-dimensional representation of electrostatic physics was formulated, where variables associated with the field were set to remain invariable in the stationary regime. This approach was implemented to ensure accurate representation and analysis of the electrostatic phenomena. Furthermore, as previously declared, the mesh settings for the simulation were configured in a ''finer'' to enhance the level of detail and accuracy in the results. Figure 4 displays the simulated concave electrode along with its respective dimensions. Figure 5 presents a 3D depiction of the electrode arrangement, the grid-like model of the sensor based on capacitance, and the electric potential (voltage) at the electrode surface. Additionally, the fluid apparatuses were
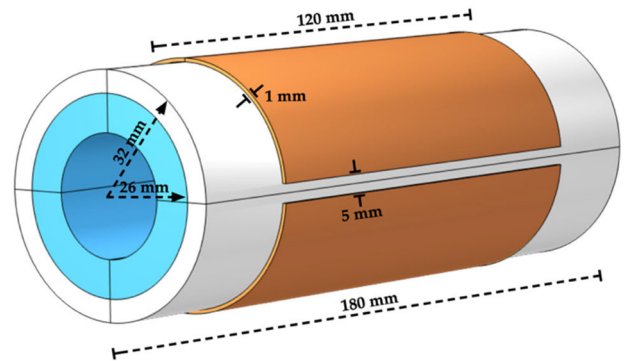

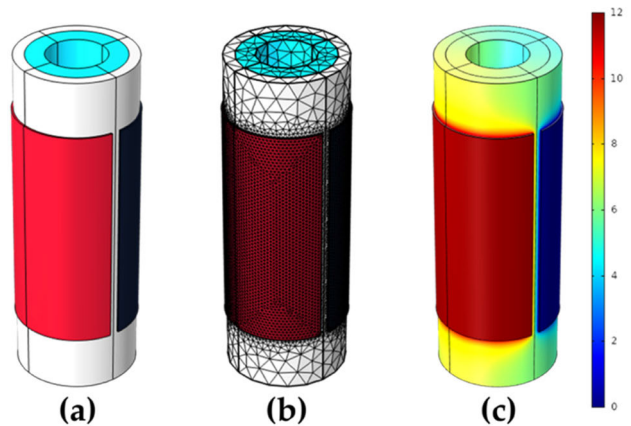**FIGURE 4.** The virtual concave sensor implemented in COMSOL software.

FIGURE 5. The modeled concave electrode: (a) Visualizing the 3D electrode structure, (b) Networked model representation, and (c) Electric field strength (voltage) distribution on sensor surface.

decomposed into 16911 3D basics using Finite Element Method (FEM).

B. MODELING AND ANALYZING A RING ELECTRODE IN COMSOL MULTIPHYSICS

Within this portion, the ring electrode was modeled using the COMSOL Multiphysics software. Similar considerations and factors that were mentioned for the concave sensor were also taken into account for the simulation of the ring sensor. Figure 6 depicts the simulated ring sensor. Furthermore, as demonstrated for the concave sensor, Figure 7 presents a three-dimensional depiction of the electrode arrangement, the grid-like model of the sensor based on capacitance, and the electric potential (voltage) at the electrode surface. The fluid components were decomposed into 16209 three-dimensional basics using the Finite Element Method (FEM).

C. MODELING AND ANALYZING A TRFLC ELECTRODE IN COMSOL MULTIPHYSICS

Within this portion, the TRFLC electrode was modeled using the COMSOL simulation platform. Similar considerations and factors that were mentioned for the concave and ring sensors were also taken into account for the simulation of the TRFLC sensor. The simulated TRFLC sensor is depicted in Figure 8. Additionally, in a manner similar to the concave
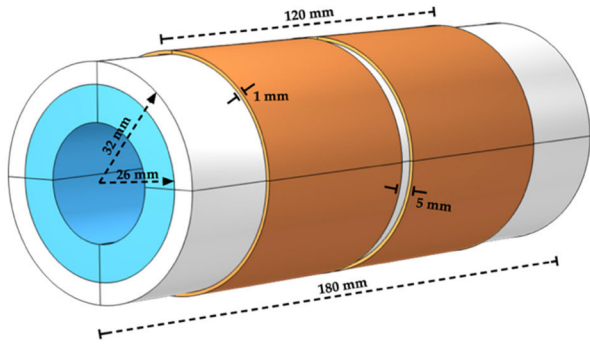
FIGURE 6. The virtual ring sensor implemented in COMSOL software.

FIGURE 7. The modeled ring electrode: (a) Visualizing the 3D electrode structure, (b) Networked model representation, and (c) Electric field strength (voltage) distribution on sensor surface.

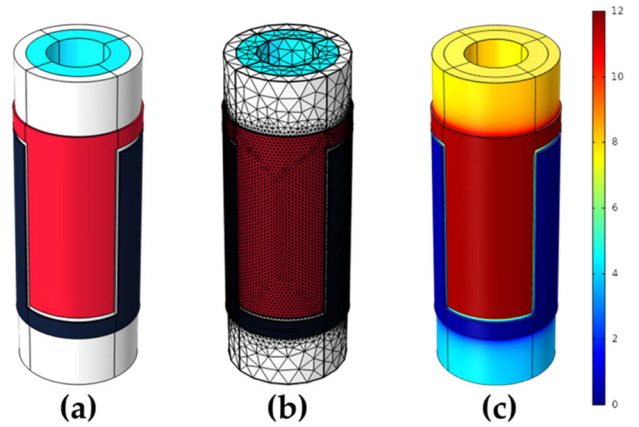**FIGURE 8.** The virtual TRFLC sensor implemented in COMSOL software.

FIGURE 9. The modeled TRFLC electrode: (a) Visualizing the 3D electrode structure, (b) Networked model representation, and (c) Electric field strength (voltage) distribution on sensor surface.
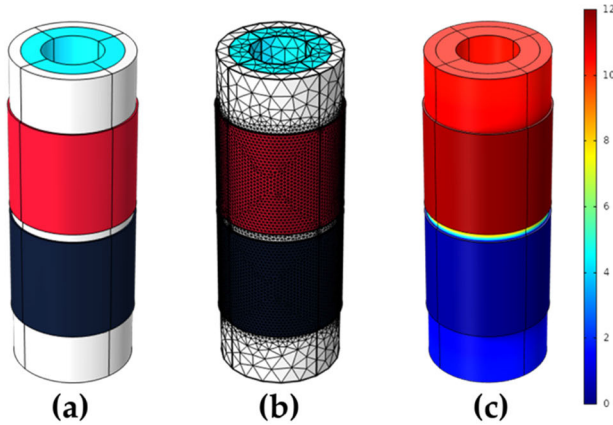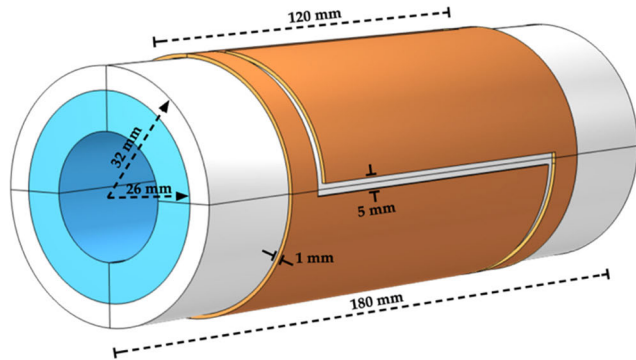
three sensors, providing a comprehensive overview of their respective outcomes.

IV. ARTIFICIAL NEURAL NETWORK

Artificial intelligence (AI) has gained widespread application through numerous activities, including medical aid, pecuniary matters, merchandise, freight, and pedagogy, among others. The application of AI extends to the analysis of medical images, disease diagnosis, and personalized treatment planning. AI-powered systems have the potential to aid radiologists in detecting anomalies in medical examinations, leading to more precise recognition. Moreover, AI can forecast the advancement of diseases and facilitate the development of tailored treatment plans for individual patients. Additionally, AI can be employed to customize shopping participation, provide product recommendations, and enhance logistics network operations. By leveraging AI algorithms, businesses can tailor the shopping experience for individual customers, offering personalized recommendations based on their preferences and previous behavior. Furthermore, AI can analyze supply chain data to enhance operational efficiency, optimize inventory management, and streamline logistics processes, ultimately improving overall supply chain performance. Moreover, AI can play a crucial role in enhancing safety, optimizing traffic flow, and enabling automated driving. Through advanced algorithms and real-time data analysis, AI systems can contribute to the development of intelligent transportation systems. These systems can improve road safety by detecting potential hazards, predicting traffic patterns, and optimizing traffic signals to ensure smoother traffic flow. Furthermore, AI technologies are at the forefront of self-driving vehicles, enabling autonomous driving capabilities and revolutionizing the future of transportation. Additionally, AI mayhap leveraged to customize training experiences, recognize areas where scholars require assistance, and develop customized education strategies. AI-powered systems can investigate scholar achievement data to pinpoint parts where scholars may be

and ring sensors, Figure 9 provides a comprehensive representation of the TRFLC sensor. This includes a detailed 3D visualization of the electrode diagram, a meticulously meshed model of the capacitance-based sensor, and a clear illustration of the electrical potential (voltage) distribution on the surface of the electrodes. These visualizations contribute to a better understanding of the sensor's structure and the electrical characteristics associated with it. Using FEM, the fluid components were decomposed into 17,479 three-dimensional fundamentals. Table 2 presents the results obtained from all

TABLE 2. The result obtained from simulated sensors.

Fluid Phase	Phase void ratio	εr	Concave (pF)	Ring (pF)	TRFLC (pF)
Crude oil	0.00	2.00	10.846	6.4637	20.449
Crude oil	0.05	2.00	10.767	6.4481	20.440
Crude oil	0.10	2.00	10.690	6.4323	20.422
Crude oil	0.15	2.00	10.626	6.4179	20.401
Crude oil	0.20	2.00	10.553	6.4018	20.371
Crude oil	0.25	2.00	10.482	6.3844	20.333
Crude oil	0.30	2.00	10.414	6.3651	20.290
Crude oil	0.35	2.00	10.348	6.3476	20.241
Crude oil	0.40	2.00	10.274	6.3259	20.191
Crude oil	0.45	2.00	10.202	6.3058	20.111
Crude oil	0.50	2.00	10.133	6.285	20.038
Crude oil	0.55	2.00	10.054	6.2591	19.957
Crude oil	0.60	2.00	9.9862	6.2296	19.866
Crude oil	0.65	2.00	9.9033	6.2062	19.767
Crude oil	0.70	2.00	9.832	6.1778	19.675
Crude oil	0.75	2.00	9.7556	6.1456	19.563
Crude oil	0.80	2.00	9.6791	6.1154	19.460
Crude oil	0.85	2.00	9.5829	6.0747	19.306
Crude oil	0.90	2.00	9.4801	6.0302	19.156
Crude oil	0.95	2.00	9.3912	5.9895	19.014
Crude oil	1.00	2.00	9.3221	5.9557	18.895
Oil	0.00	2.20	11.127	6.5603	20.730
Oil	0.05	2.20	11.033	6.5421	20.720
Oil	0.10	2.20	10.940	6.5233	20.699
Oil	0.15	2.20	10.863	6.5062	20.674
Oil	0.20	2.20	10.776	6.4869	20.638
Oil	0.25	2.20	10.691	6.4661	20.593
Oil	0.30	2.20	10.609	6.4432	20.541
Oil	0.35	2.20	10.531	6.4222	20.483
Oil	0.40	2.20	10.443	6.3963	20.422
Oil	0.45	2.20	10.356	6.3724	20.330
Oil	0.50	2.20	10.276	6.3472	20.243
Oil	0.55	2.20	10.184	6.3167	20.147
Oil	0.60	2.20	10.102	6.2821	20.040
Oil	0.65	2.20	10.006	6.2537	19.925
Oil	0.70	2.20	9.9213	6.2197	19.814
Oil	0.75	2.20	9.8322	6.1822	19.684
Oil	0.80	2.20	9.7423	6.1461	19.561
Oil	0.85	2.20	9.6297	6.0979	19.383

TABLE 2. *(Continued.)* The result obtained from simulated sensors.

Fluid Phase	Phase void ratio	εr	Concave (pF)	Ring (pF)	TRFLC (pF)
Oil	0.90	2.20	9.5116	6.0461	19.208
Oil	0.95	2.20	9.4075	5.9979	19.041
Oil	1.00	2.20	9.326	5.9576	18.901
Diesel fuel	0.00	2.40	11.410	6.6551	21.001
Diesel fuel	0.05	2.40	11.291	6.6343	20.989
Diesel fuel	0.10	2.40	11.182	6.6125	20.965
Diesel fuel	0.15	2.40	11.093	6.5928	20.937
Diesel fuel	0.20	2.40	10.992	6.5703	20.895
Diesel fuel	0.25	2.40	10.893	6.5462	20.843
Diesel fuel	0.30	2.40	10.798	6.5197	20.783
Diesel fuel	0.35	2.40	10.708	6.4954	20.716
Diesel fuel	0.40	2.40	10.606	6.4654	20.644
Diesel fuel	0.45	2.40	10.507	6.4376	20.541
Diesel fuel	0.50	2.40	10.414	6.4081	20.441
Diesel fuel	0.55	2.40	10.310	6.3731	20.331
Diesel fuel	0.60	2.40	10.214	6.3335	20.208
Diesel fuel	0.65	2.40	10.106	6.3002	20.076
Diesel fuel	0.70	2.40	10.007	6.2608	19.948
Diesel fuel	0.75	2.40	9.9061	6.218	19.800
Diesel fuel	0.80	2.40	9.8032	6.1762	19.659
Diesel fuel	0.85	2.40	9.6749	6.1207	19.456
Diesel fuel	0.90	2.40	9.5421	6.0617	19.258
Diesel fuel	0.95	2.40	9.4233	6.0061	19.067
Diesel fuel	1.00	2.40	9.3297	5.9597	18.908
Gasoline	0.00	2.70	11.793	6.7941	21.388
Gasoline	0.05	2.70	11.663	6.7694	21.374
Gasoline	0.10	2.70	11.532	6.7433	21.346
Gasoline	0.15	2.70	11.425	6.7197	21.312
Gasoline	0.20	2.70	11.304	6.6926	21.263
Gasoline	0.25	2.70	11.185	6.6636	21.201
Gasoline	0.30	2.70	11.070	6.6317	21.129
Gasoline	0.35	2.70	10.963	6.6025	21.050
Gasoline	0.40	2.70	10.841	6.5665	20.962
Gasoline	0.45	2.70	10.724	6.5331	20.843
Gasoline	0.50	2.70	10.613	6.4973	20.724
Gasoline	0.55	2.70	10.491	6.4558	20.595
Gasoline	0.60	2.70	10.376	6.4088	20.448
Gasoline	0.65	2.70	10.249	6.3683	20.294
Gasoline	0.70	2.70	10.132	6.3209	20.140

facing challenges. Based on this analysis, personalized learning materials can be provided to students, aiding them in improving their understanding and skills. This personalized approach to education has the potential to enhance student

TABLE 2. *(Continued.)* The result obtained from simulated sensors.

Fluid Phase	Phase void ratio	εr	Concave (pF)	Ring (pF)	TRFLC (pF)
Gasoline	0.75	2.70	10.013	6.2705	19.968
Gasoline	0.80	2.70	9.8912	6.2203	19.800
Gasoline	0.85	2.70	9.7402	6.1541	19.563
Gasoline	0.90	2.70	9.5861	6.0846	19.331
Gasoline	0.95	2.70	9.4461	6.0182	19.106
Gasoline	1.00	2.70	9.3352	5.9626	18.917
water	0.00	81.00	28.341	19.516	34.638
water	0.05	81.00	28.073	19.253	34.582
water	0.10	81.00	27.771	18.950	34.506
water	0.15	81.00	27.498	18.678	34.429
water	0.20	81.00	27.161	18.346	34.326
water	0.25	81.00	26.795	17.992	34.204
water	0.30	81.00	26.389	17.598	34.060
water	0.35	81.00	25.991	17.228	33.908
water	0.40	81.00	25.480	16.760	33.719
water	0.45	81.00	24.972	16.317	33.489
water	0.50	81.00	24.391	15.813	33.229
water	0.55	81.00	23.730	15.266	32.924
water	0.60	81.00	22.967	14.641	32.543
water	0.65	81.00	22.140	14.015	32.109
water	0.70	81.00	21.178	13.298	31.577
water	0.75	81.00	20.164	12.579	30.950
water	0.80	81.00	18.957	11.762	30.151
water	0.85	81.00	17.246	10.659	28.831
water	0.90	81.00	15.317	9.4787	27.072
water	0.95	81.00	12.971	8.0876	24.405
water	1.00	81.00	9.3406	5.9597	19.069

engagement and academic outcomes [48], [52]. The notion of Artificial Neural Networks (ANN) has occupied a prominent role in the realm of artificial intelligence for several decades, starting from the 1980s. Fundamentally, ANN aims to emulate and replicate the complex information processing observed in the neural networks of the human brain. This emulation leads to the creation of a simplified model that can be flexibly configured into various network setups by utilizing different connections [53]. ANNs, which are composed of interconnected neurons, are widely recognized as among the most precise approaches in mathematics. ANNs have proven outstanding achievements across diverse domains, like pattern identification, machine learning, and data analysis. Their ability to model complex relationships and adapt to changing inputs makes them valuable tools for solving

mathematical problems with high precision and accuracy. According to [54], ANN is a dependable method within the field of soft computing, capable of tackling complex problems. Every individual node within the network is linked to a particular output function referred to as the activation function. Concurrently, the connections that interconnect these nodes are characterized by weight factors, representing the intensity of signal transmission through these links. It is these weight values that play a crucial role in the artificial neural network's memory management [55]. Neurons, which serve as fundamental computing components, can be generated as single or multiple layers [56]. Artificial Neural Networks (ANNs) are capable of making predictions, and a wide range of ANNs have been developed, each with unique characteristics. Among them, the multilayer perceptron (MLP) stands out as one of the most effective ANNs with diverse applications. Therefore, researchers often choose MLP when seeking rapid and accurate results [57]. This paradigm employs two distinct groups of data: the training group and the testing group. The training group consists of a finite quantity of precise data, which is utilized to train the network. On the other hand, the testing group contains data that the network has not previously encountered and serves the purpose of evaluating the network's accuracy and performance [58]. Two MLP networks were established, incorporating input data acquired from the capacitance measurements of two distinct sensor configurations. The first network utilized data from the concave and TRFLC sensors, while the second network integrated data from the TRFLC and ring sensors. In the pursuit of identifying the most suitable networks with the lowest mean absolute error, various networks were evaluated and compared based on their distinct characteristics, including varying numbers of neurons, epochs, hidden layers, and even various kinds of activation functions. After extensive investigation, the networks that performed the best and minimized the mean absolute error were selected. After persistent investigation and iterative modifications to different components of the networks, the proposed networks were eventually selected. The rigorous evaluation process involved scrutinizing various aspects and making repeated adjustments until arriving at the final selection of the most suitable network configuration. The MLP networks illustrated in Figure 10 were designed with two input nodes and a single output per network. Table 2 presents the statistics acquired from the integrated sensors for different liquids, encompassing and water ($\varepsilon r = 81$), gasoline ($\varepsilon r = 2.7$), diesel fuel ($\varepsilon r = 2.4$), oil ($\varepsilon r = 2.2$), and crude oil ($\varepsilon r = 2$). With the aid of the COMSOL FEA program, 105 simulations were carried out for the specified fluids, varying the volume percentages from 0 to 1 in increments of 0.05. Seventy percent (73) of the simulations were chosen randomly to be used as training data, while the remaining 30% (32) were kept aside for testing purposes. After assessing numerous networks with varying digits of neurons and layers, the ideal arrangement was obtained.
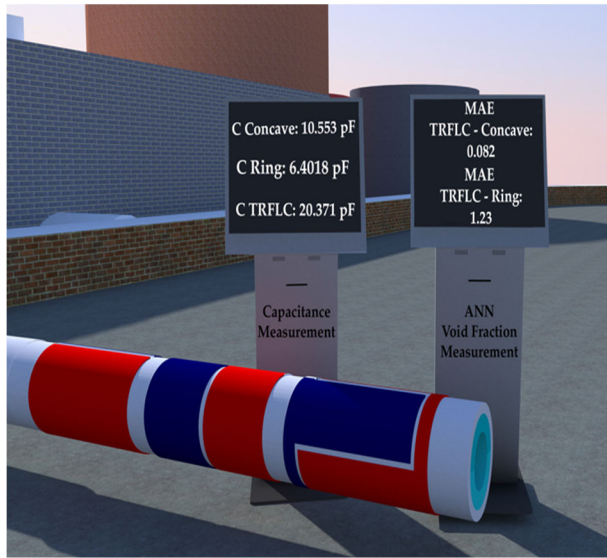
FIGURE 10. Illustration of forecasting the volume percentage utilizing the suggested ANN.

TABLE 3. Proposed ANN model configuration.

Sensors	Concave-TRFLC	Ring-TRFLC
Neural Network	MLP	MLP
Neurons in the input layer	3	3
Neurons in the hidden layer	5	3
Neurons in the output layer	1	1
Number of epochs	500	200
Activation function of neurons in hidden layers	Tansig	Tansig
Activation function of neurons in input and output layers	Purelin	Purelin
Method of training	Levenberg–Marquardt [59,60]	Levenberg–Marquardt [59,60]

Table 3 contains the details of the network model's characteristics.

V. RESULT AND DISCUSSION

In Figure 10, the schematic view of forecasting the void fraction using the suggested ANN was shown. As mentioned earlier, there were 105 groups of statistics available from simulations. Out of these, 70% of them were utilized for training, while the residual 30% were employed for testing purposes. The data was randomly split between the training and testing sets. A thorough investigation was conducted of various networks to select the best architecture. Combinations with high error rates were eliminated, and the outputs of combinations with low errors were regarded as new independent variables. This process was iteratively pursued until the achievement of the final output with the minimum error rate. In the results obtained from the presented ANN, two crucial factors are considered: real and predicted data. Real data were generated

through simulation, while the proposed neural network provided predicted data. Figure 11a shows the regression graph for the training data set, while Figure 11b displays the regression graph for the testing data set from the TRFLC-Ring network. Figure 12a represents the regression graph for the training data set from the TRFLC-Concave network, while Figure 12b displays the regression graph for the testing data set from the same network. The depicted image demonstrates the proximity of the real data to the predicted data generated by both networks. In order to assess the precision of the proposed MLP models, Equation (3) was utilized to compute the mean absolute error (MAE). Equation (4) was utilized to calculate the mean relative error percentage (MRE%). In the specified equation, "N" refers to the total quantity of observations, The terms X(Sim) and X(Pred) represent the values obtained from simulation (using COMSOL simulation platform) and estimation (using MLP), respectively. Regression is a statistical method employed to assess the strength of the relationship between two variables. It helps determine the degree of association or dependency between these variables, allowing us to understand how changes in one variable may impact the other. The Mean Absolute Error (MAE) and Mean Relative Error percentage (MRE%).for the training and testing TRFLC-Ring datasets were 0.031, 0.12% and 0.038, 0.122% proportionately, while for the training and testing TRFLC-Concave datasets, the MAE and MRE% values were 0.004, 0.021% and 0.008, 0.038% proportionately. Compared to earlier relevant research, recent investigations reported in references [30], [32], [33], and [35] explored the two-phase flow regimes. These studies revealed MAE values of 1.74, 1.28, 4.86 and 0.38 respectively. Thanks to the utilization of an optimized combined sensor, a more fitting model, and a higher number of inputs in comparison to the study mentioned, the current network demonstrated markedly superior performance.

$$MAE = \frac{1}{N} \sum_{i=1}^{z} |x_i(sim) - x_i(pred)| \quad (3)$$

$$MRE\% = 100 \times \frac{1}{N} \sum_{i=1}^{N} |\frac{x_i(Sim) - x_i(Pred)}{x_i(Sim)}| \quad (4)$$
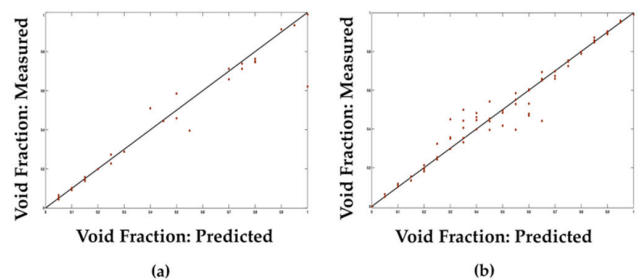

FIGURE 11. Scatter plots illustrating the regression outcomes of TRFLC-Ring for simulated versus predicted results, shown for (a) the training dataset and (b) the testing dataset.

The superiority of the proposed TRFLC-Concave MLP model in accurately measuring void fraction is striking,
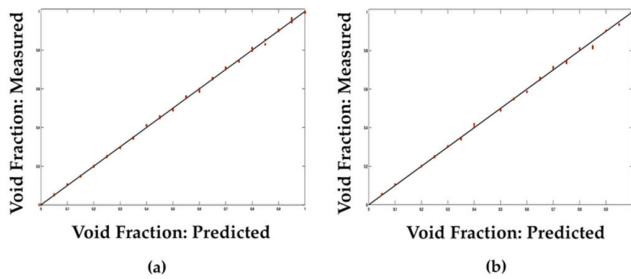
FIGURE 12. Scatter plots illustrating the regression outcomes of TRFLC-Ring for simulated versus predicted results, shown for (a) the training dataset and (b) the testing dataset.

evident through its remarkable precision and considerably reduced mean absolute error when juxtaposed with the TRFLC-Ring combination. This impressive performance can be attributed to the heightened overall sensitivity exhibited by both the concave and TRFLC models, a fact underscored by the data presented in Table 2. The significant achievement of evaluating the relationship between two variables was made possible through the use of an ANN in conjunction with combined capacitance-based sensors. It is worth noting that the small Mean Absolute Error (MAE) values for both the training and testing sets indicate the high accuracy and correctness of the proposed Artificial Neural Network (ANN) in producing precise results. Upon examining the error ratio, it becomes evident that the errors are lower, thereby confirming the validity of the well-trained ANN model, which does not experience under-fitting or over-fitting issues. The minimal errors in the training set indicate the absence of under-fitting problems and the model's precision. Additionally, as depicted in Figure 12, there were no signs of underfitting or overfitting observed, affirming the reliability and credibility of the presented model.

VI. CONCLUSION

The primary aim of this investigation was to Precisely forecast the gas fraction in annular biphasic fluid motion, independent of the particular liquid phases present. To accomplish this goal, an MLP ANN was used. To facilitate the provision of data for the suggested ANN, novel merged capacitive sensors were utilized. The data for the proposed ANN was obtained from a grouping of sensors, including a concave sensor, a ring sensor, and a TRFLC sensor connected in series. Both of these sensors were intended and pretended using the COMSOL Multiphysics program. The investigation involved the study of 5 special types of liquids: water, gasoline, diesel fuel, oil, and crude oil. Simulations were conducted with 21 repetitions for each liquid, covering specific void fractions, starting from 0 and increasing by 0.05 each time. As a result, A total of 105 data sets were gathered to both train and test the demonstrated network. Each of the ANN networks presented in the study was designed with two entries, representing the results attained from the TRFLC-Concave and TRFLC-Ring sensors. These inputs were generated by

simulating the sensors in COMSOL Multiphysics. Indeed, each of these ANN networks was configured to have one outturn, which represented the forecast void fraction. The Mean Absolute Error (MAE) and Mean Relative Error percentage (MRE%) on the TRFLC-Ring datasets were 0.031, 0.12% for training and 0.038, 0.122% for testing, respectively. On the TRFLC-Concave datasets, the corresponding MAE and MRE% values for training and testing were 0.004, 0.021% and 0.008, 0.038% respectively. By utilizing the proposed novel metering structure, it is possible to accurately predict the gas fraction of any annular biphasic fluid motion, irrespective of the specific liquid phases involved. In this context, the performance and effectiveness of an MLP ANN were thoroughly considered. The primary objective of the investigation was to achieve precise void fraction prediction, irrespective of the type of liquid present inner part of the tube. Both an MLP and a capacitive sensor were utilized in order to reach the desired outcome. These tools were utilized to accurately predict the void fraction in the presence of various types of liquids inside the pipe. For future research, considering the use of other types of ANNs, and soft computing methods could be beneficial. Additionally, exploring a combination of sensors with different shapes could also be considered to enhance the accuracy and robustness of the void fraction prediction system.

REFERENCES

[1] H. Karimi and M. Boostani, "Heat transfer measurements for oil-water flow of different flow patterns in a horizontal pipe," *Experim. Thermal Fluid Sci.*, vol. 75, pp. 35–42, Jul. 2016.

[2] E. Nazemi, G. H. Roshani, S. A. H. Feghhi, S. Setayeshi, E. E. Zadeh, and A. Fatehi, "Optimization of a method for identifying the flow regime and measuring void fraction in a broad beam gamma-ray attenuation technique," *Int. J. Hydrogen Energy*, vol. 41, no. 18, pp. 7438–7444, May 2016.

[3] R. N. Steven, "Wet gas metering with a horizontally mounted Venturi meter," *Flow Meas. Instrum.*, vol. 12, nos. 5–6, pp. 361–372, Jan. 2002.

[4] D. Wang, F.-C. Liang, Z.-Q. Peng, Y.-G. Wang, and Z.-H. Lin, "Gas-liquid two-phase flow measurements by full stream batch sampling," *Int. J. Multiphase Flow*, vol. 40, pp. 113–125, Apr. 2012.

[5] M. Banowski, M. Beyer, L. Szalinski, D. Lucas, and U. Hampel, "Comparative study of ultrafast X-ray tomography and wire-mesh sensors for vertical gas-liquid pipe flows," *Flow Meas. Instrum.*, vol. 53, pp. 95–106, Mar. 2017.

[6] C. M. Salgado, R. S. F. Dam, E. J. A. Puertas, and W. L. Salgado, "Calculation of volume fractions regardless scale deposition in the oil industry pipelines using feed-forward multilayer perceptron artificial neural network and MCNP6 code," *Appl. Radiat. Isot.*, vol. 185, Jul. 2022, Art. no. 110215.

[7] A. M. Iliyasu, D. K. Bagaudinovna, A. S. Salama, G. H. Roshani, and K. Hirota, "A methodology for analysis and prediction of volume fraction of two-phase flow using particle swarm optimization and group method of data handling neural network," *Mathematics*, vol. 11, no. 4, p. 916, Feb. 2023.

[8] S. Al-lababidi, A. Addali, H. Yeung, D. Mba, and F. Khan, "Gas void fraction measurement in two-phase gas/liquid slug flow using acoustic emission technology," *J. Vib. Acoust.*, vol. 131, no. 6, pp. 501–507, Dec. 2009.

[9] C. G. Xie, A. L. Stott, A. Plaskowski, and M. S. Beck, "Design of capacitance electrodes for concentration measurement of two-phase flow," *Meas. Sci. Technol.*, vol. 1, no. 1, pp. 65–78, Jan. 1990.

[10] M. Abdulkadir, V. Hernandez-Perez, I. S. Lowndes, B. J. Azzopardi, and E. T. Brantson, "Detailed analysis of phase distributions in a vertical riser using wire mesh sensor (WMS)," *Experim. Thermal Fluid Sci.*, vol. 59, pp. 32–42, Nov. 2014.

[11] S. Koyama, J. Lee, and R. Yonemoto, "An investigation on void fraction of vapor-liquid two-phase flow for smooth and microfin tubes with R134a at adiabatic condition," *Int. J. Multiphase Flow*, vol. 30, no. 3, pp. 291–310, Mar. 2004.

[12] M. Demori, V. Ferrari, D. Strazza, and P. Poesio, "A capacitive sensor system for the analysis of two-phase flows of oil and conductive water," *Sens. Actuators A, Phys.*, vol. 163, no. 1, pp. 172–179, Sep. 2010.

[13] D. Strazza, M. Demori, V. Ferrari, and P. Poesio, "Capacitance sensor for hold-up measurement in high-viscous-oil/conductive-water core-annular flows," *Flow Meas. Instrum.*, vol. 22, no. 5, pp. 360–369, Oct. 2011.

[14] Z. An, J. Ningde, Z. Lusheng, and G. Zhongke, "Liquid holdup measurement in horizontal oil-water two-phase flow by using concave capacitance sensor," *Measurement*, vol. 49, pp. 153–163, Mar. 2014.

[15] J. Ortiz and V. Masek, "Cyclonic capacitive sensor for multiphase composition measurement," *Sensors Transducers*, vol. 191, no. 8, pp. 1–11, Aug. 2015.

[16] L. S. Zhai, N. D. Jin, Z. K. Gao, A. Zhao, and L. Zhu, "Cross-correlation velocity measurement of horizontal oil-water two-phase flow by using parallel-wire capacitance probe," *Experim. Thermal Fluid Sci.*, vol. 53, pp. 277–289, Feb. 2014.

[17] L. Zhai, N. Jin, Z. Gao, and Z. Wang, "Liquid holdup measurement with double helix capacitance sensor in horizontal oil-water two-phase flow pipes," *Chin. J. Chem. Eng.*, vol. 23, no. 1, pp. 268–275, Jan. 2015.

[18] J. Li, M. Kong, C. Xu, S. Wang, and Y. Fan, "An integrated instrumentation system for velocity, concentration and mass flow rate measurement of solid particles based on electrostatic and capacitance sensors," *Sensors*, vol. 15, no. 12, pp. 31023–31035, Dec. 2015.

[19] J. Tollefsen and E. A. Hammer, "Capacitance sensor design for reducing errors in phase concentration measurements," *Flow Meas. Instrum.*, vol. 9, no. 1, pp. 25–32, Mar. 1998.

[20] A. Jaworek and A. Krupa, "Gas/liquid ratio measurements by RF resonance capacitance sensor," *Sens. Actuators A, Phys.*, vol. 113, no. 2, pp. 133–139, Jul. 2004.

[21] E. dos Reis and D. da Silva Cunha, "Experimental study on different configurations of capacitive sensors for measuring the volumetric concentration in two-phase flows," *Flow Meas. Instrum.*, vol. 37, pp. 127–134, Jun. 2014.

[22] A. A. Kendoush and Z. A. Sarkis, "Improving the accuracy of the capacitance method for void fraction measurement," *Exp. Thermal Fluid Sci.*, vol. 11, no. 4, pp. 321–326, Nov. 1995.

[23] M. S. A. Abouelwafa and E. J. M. Kendall, "The use of capacitance sensors for phase percentage determination in multiphase pipelines," *IEEE Trans. Instrum. Meas.*, vol. IM-29, no. 1, pp. 24–27, Mar. 1980.

[24] H. Ahmed, "Capacitance sensors for void-fraction measurements and flow-pattern identification in air-oil two-phase flow," *IEEE Sensors J.*, vol. 6, no. 5, pp. 1153–1163, Oct. 2006.

[25] M. Roshani, G. T. T. Phan, E. Nazemi, E. Eftekhari-Zadeh, N.-H. Phan, E. Corniani, H.-N. Tran, V. H. Duong, and G. H. Roshani, "Performance comparison of capacitance-based flowmeter with gamma-ray attenuation-based two-phase flowmeter for determining volume fractions in an annular flow regime's components," *Eur. Phys. J. Plus*, vol. 136, no. 2, pp. 24–27, Feb. 2021.

[26] X. Wang, Y. Chen, B. Wang, K. Tang, and H. Hu, "Sectional void fraction measurement of gas-water two-phase flow by using a capacitive array sensor," *Flow Meas. Instrum.*, vol. 74, Aug. 2020, Art. no. 101788.

[27] A. Krupa, M. Lackowski, and A. Jaworek, "Capacitance sensor for measuring void fraction in small channels," *Measurement*, vol. 175, Apr. 2021, Art. no. 109046.

[28] D. He, S. Chen, and B. Bai, "Void fraction measurement of stratified gas-liquid flow based on multi-wire capacitance probe," *Experim. Thermal Fluid Sci.*, vol. 102, pp. 61–73, Apr. 2019.

[29] M. H. Shahsavari, A. Veisi, G. H. Roshani, E. Eftekhari-Zadeh, and E. Nazemi, "An experimental and simulation study for comparison of the sensitivity of different non-destructive capacitive sensors in a stratified two-phase flow regime," *Electronics*, vol. 12, no. 6, p. 1284, Mar. 2023.

[30] A. M. Iliyasu, F. Fouladinia, A. S. Salama, G. H. Roshani, and K. Hirota, "Intelligent measurement of void fractions in homogeneous regime of two phase flows independent of the liquid phase density changes," *Fractal Fractional*, vol. 7, no. 2, p. 179, Feb. 2023.

[31] S. Rushd, U. Gazder, H. J. Qureshi, and M. Arifuzzaman, "Advanced machine learning applications to viscous oil-water multi-phase flow," *Appl. Sci.*, vol. 12, no. 10, p. 4871, May 2022.

[32] A. Veisi, M. H. Shahsavari, G. H. Roshani, E. Eftekhari-Zadeh, and E. Nazemi, "Experimental study of void fraction measurement using a capacitance-based sensor and ANN in two-phase annular regimes for different fluids," *Axioms*, vol. 12, no. 1, p. 66, Jan. 2023.

[33] A. M. Mayet, G. E. Ilyinichna, F. Fouladinia, M. S. Daoud, V. P. T. Ijyas, N. K. Shukla, M. S. Habeeb, and H. H. Alhashim, "An artificial neural network and a combined capacitive sensor for measuring the void fraction independent of temperature and pressure changes for a two-phase homogeneous fluid," *Flow Meas. Instrum.*, vol. 93, Oct. 2023, Art. no. 102406.

[34] A. M. Mayet, K. S. Nurgalieva, A. A. Al-Qahtani, I. M. Narozhnyy, H. H. Alhashim, E. Nazemi, and I. M. Indrupskiy, "Proposing a high-precision petroleum pipeline monitoring system for identifying the type and amount of oil products using extraction of frequency characteristics and a MLP neural network," *Mathematics*, vol. 10, no. 16, p. 2916, Aug. 2022.

[35] R. M. A. Qaisi, F. Fouladinia, A. M. Mayet, J. W. G. Guerrero, H. Loukil, M. R. Raja, M. A. Muqeet, and E. Eftekhari-Zadeh, "Intelligent measuring of the volume fraction considering temperature changes and independent pressure variations for a two-phase homogeneous fluid using an 8-electrode sensor and an ANN," *Sensors*, vol. 23, no. 15, p. 6959, Aug. 2023.

[36] R. B. Y. Syah, A. Veisi, Z. A. Hasibuan, M. A. Al-Fayoumi, M. S. Daoud, and E. Eftekhari-Zadeh, "A novel smart optimized capacitance-based sensor for annular two-phase flow metering with high sensitivity," *IEEE Access*, vol. 11, pp. 60709–60716, 2023, doi: 10.1109/ACCESS.2023.3281754.

[37] A. M. Mayet, S. M. Alizadeh, K. S. Nurgalieva, R. Hanus, E. Nazemi, and I. M. Narozhnyy, "Extraction of time-domain characteristics and selection of effective features using correlation analysis to increase the accuracy of petroleum fluid monitoring systems," *Energies*, vol. 15, no. 6, p. 1986, Mar. 2022.

[38] M. Elbes, S. Alzubi, T. Kanan, A. Al-Fuqaha, and B. Hawashin, "A survey on particle swarm optimization with emphasis on engineering and network applications," *Evol. Intell.*, vol. 12, no. 2, pp. 113–129, Jun. 2019, doi: 10.1007/s12065-019-00210-z.

[39] G. H. Roshani, E. Nazemi, and M. M. Roshani, "Intelligent recognition of gas-oil-water three-phase flow regime and determination of volume fraction using radial basis function," *Flow Meas. Instrum.*, vol. 54, pp. 39–45, Apr. 2017.

[40] A. D. N. Wrasse, E. N. D. Santos, M. J. D. Silva, H. Wu, and C. Tan, "Capacitive sensors for multiphase flow measurement: A review," *IEEE Sensors J.*, vol. 22, no. 22, pp. 21391–21409, Nov. 2022.

[41] Z. Huang, H. Wang, and X. Zhang, "Design of capacitance sensor for two phase flow monitoring based on finite element models," *Int. J. Comput. Appl. Technol.*, vol. 62, no. 4, p. 348, 2020.

[42] Z. Xu, F. Wu, X. Wang, and Y. Li, "Measurement of gas-oil two-phase flow patterns by using CNN algorithm based on dual ECT sensors with Venturi tube," *Sensors*, vol. 20, no. 4, p. 1200, Feb. 2020.

[43] A. D. N. Wrasse, T. P. Vendruscolo, E. N. Santos, F. C. Castaldo, R. E. M. Morales, and M. J. da Silva, "Capacitive direct-imaging sensor for two-phase flow visualization," in *Proc. IEEE SENSORS*, Oct. 2016, pp. 1–3.

[44] L. Zhai, R. Liu, H. Zhang, and N. Jin, "Complex admittance detection of horizontal oil-water two-phase flows using a capacitance sensor," *IEEE Sensors J.*, vol. 19, no. 17, pp. 7489–7498, Sep. 2019.

[45] M. Kim, K. Komeda, J. Jeong, T. Oinuma, T. Sato, and K. Saito, "Optimizing calibration for a capacitance-based void fraction sensor with asymmetric electrodes under horizontal flow in a smoothed circular macro-tube," *Sensors*, vol. 22, no. 9, p. 3511, May 2022.

[46] S. M. Salehi, H. Karimi, A. A. Dastranj, and R. Moosavi, "Twin rectangular fork-like capacitance sensor to flow regime identification in horizontal co-current gas-liquid two-phase flow," *IEEE Sensors J.*, vol. 17, no. 15, pp. 4834–4842, Aug. 2017, doi: 10.1109/JSEN.2017.2708663.

[47] C. E. Brennen, *Fundamentals of Multiphase Flow*. New York, NY, USA: Cambridge Univ. Press, 2005.

[48] A. Esteva, A. Robicquet, B. Ramsundar, V. Kuleshov, M. DePristo, K. Chou, C. Cui, G. Corrado, S. Thrun, and J. Dean, "A guide to deep learning in healthcare," *Nature Med.*, vol. 25, pp. 24–29, Jan. 2019.

[49] J. Li, Z. Yang, W. Li, and Y. Li, "A survey on deep learning in finance," *Neural Comput. Appl.*, pp. 3385–3407, 2020.

[50] E. Rahimi and T. Nguyen, "Retail analytics: A review and future research directions," *J. Retailing Consum. Services*, pp. 170–181, 2018.
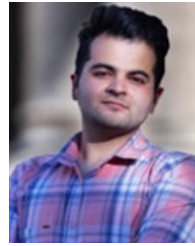
[51] Z. Zhang, J. Liu, Z. Shen, and J. Huang, "A survey on deep learning for traffic prediction," *IEEE Trans. Intell. Transp. Syst.*, vol. 99, pp. 3536–3553, 2019.

[52] V. Kovanovic, S. Joksimovic, D. Gašševic, G. Siemens, and M. Hatala, "Applications of machine learning in education," *J. Educ. Technol. Soc.*, pp. 33–47, 2018.

[53] J. Dong and S. Hu, "The progress and prospects of neural network research," *Inf. Control*, vol. 26, pp. 360–368, 1997.

[54] S. Rezvan, M. J. Moradi, H. Dabiri, K. Daneshvar, M. Karakouzian, and V. Farhangi, "Application of machine learning to predict the mechanical characteristics of concrete containing recycled plastic-based materials," *Appl. Sci.*, vol. 13, no. 4, p. 2033, Feb. 2023.

[55] A. Bulsari, "Some analytical solutions to the general approximation problem for feedforward neural networks," *Neural Netw.*, vol. 6, no. 7, pp. 991–996, Jan. 1993.

[56] G. H. Roshani, S. A. H. Feghhi, A. Mahmoudi-Aznaveh, E. Nazemi, and A. Adineh-Vand, "Precise volume fraction prediction in oil-water-gas multiphase flows by means of gamma-ray attenuation and artificial neural networks using one detector," *Measurement*, vol. 51, pp. 34–41, May 2014.

[57] A. R. Gallant and H. White, "On learning the derivatives of an unknown mapping with multilayer feedforward networks," *Neural Netw.*, vol. 5, no. 1, pp. 129–138, Jan. 1992.

[58] C. M. Salgado, L. E. B. Brandão, R. Schirru, C. M. N. A. Pereira, A. X. da Silva, and R. Ramos, "Prediction of volume fractions in three-phase flows using nuclear technique and artificial neural network," *Appl. Radiat. Isot.*, vol. 67, no. 10, pp. 1812–1818, Oct. 2009.

[59] K. Levenberg, "A method for the solution of certain non-linear problems in least squares," *Quart. Appl. Math.*, vol. 2, no. 2, pp. 164–168, Jan. 1944.

[60] D. W. Marquardt, "An algorithm for least-squares estimation of nonlinear parameters," *J. Soc. Ind. Appl. Math.*, vol. 11, no. 2, pp. 431–441, Jun. 1963.

ARYAN VEISI was born in Kermanshah, Iran. He received the B.Sc. degree in electrical engineering from the Kermanshah University of Technology, Kermanshah, in 2020, where he is currently pursuing the M.Sc. degree in electrical engineering: integrated electronic circuits. His current research interests include the design and implementation of capacitance-based sensors, modeling and computing, and artificial intelligence.

HUSSAIN AL-AQRABI received the M.Sc. degree in computer networks from the University of Derby, U.K., in 2011, and the Ph.D. degree in computer science / cloud security from the University of Derby, U.K., in 2016. He has been an Assistant Professor with the Department of Computer Information Science, Higher Colleges of Technology (HCT), UAE, since 2022. Prior to joining the HCT, he worked as an Associate Professor at the University of Huddersfield beginning in 2017. He is a Fellow of the Higher Education Academy, U.K. In addition to his university education, he holds industry certifications, including EC-Council Certified Ethical Hacker and Microsoft Certified IT Professional on Windows Server, and he is also Cisco Certified in Routing and Switching. He has published over 60 publications in peer-reviewed journals, international conferences, and book series. His research interests include cyber security, cloud security, multiparty authentication, digital manufacturing, the industrial Internet of Things, artificial intelligence, distributed ledger, network security, optimisation, secure protocol development, and evaluation.

MUSTAFA A. AL-FAYOUMI received the B.Sc. degree in computer science from Yarmouk University, Irbid, Jordan, in 1988, the master's degree in computer science from The University of Jordan, Amman, Jordan, in 2003, and the Ph.D. degree in computer science from the Faculty of Science and Technology, Anglia University, U.K., in 2009. He is currently an Associate Professor of computer science and the Head of the Department of Cybersecurity, Princess Sumaya University for Technology (PSUT). His research interests include computer security, cryptography, identification and authentication, wireless and mobile networks security, e-application security, intelligent applications, intelligent threat detection, machine learning, and other related topics

MOHAMMAD SH. DAOUD received the Ph.D. degree in computer science from De Montfort University, U.K. He is currently an Associate Professor with the College of Engineering, Al Ain University, United Arab Emirates. His research interests include artificial intelligence, swarm systems, secured systems and networks, and smart applications.

HANI MAHMOUD AL-MIMI received the B.Sc. degree (Hons.) in computer science from Al-Zaytoonah University of Jordan (ZUJ), in 2001, the M.Sc. degree in computer science from The University of Jordan, in 2005, and the Ph.D. degree in computer science from Universiti Sains Malaysia (USM), in 2014. He is currently an Assistant Professor with the Faculty of Science and Information Technology, ZUJ. His research interests include computer networks, artificial intelligence, wireless and mobile networks, computer security, cyber security, and cryptography.

EHSAN EFTEKHARI-ZADEH received the B.Sc. degree in physics from the Shahid Chamran University of Ahvaz, Iran, in 2012, and the M.Sc. degree in nuclear engineering: radiation applications from Shahid Beheshti University, Tehran, Iran, in 2015. He is currently pursuing the Ph.D. degree in physics/photonics with Friedrich Schiller University Jena, Jena, Germany. He gained a few years of professional experience in the gamma irradiation industry in Iran. Since 2019, he has been a Scientific Assistant with the Institute of Optics and Quantum Electronics, Jena.

• • •